Journal of Alloys and Compounds 502 (2010) 28–37

Contents lists available at ScienceDirect

Journal of Alloys and Compounds

journal homepage: www.elsevier.com/locate/jallcom

Theoretical study on the stability, elasticity, hardness and electronic structures of W–C binary compounds

Yefei Li[a,*], Yimin Gao[a,*], Bing Xiao[b], Ting Min[a], Zijian Fan[a], Shengqiang Ma[a], Leilei Xu[c]

[a] State Key Laboratory for Mechanical Behavior of Materials, Xi'an Jiaotong University, Xi'an 710049, PR China
[b] Department of Physics and Quantum Theory Group, School of Science and Engineering, Tulane University, New Orleans, LA 70118, USA
[c] Technology Center, Tianjin Pipe (Group) Corp Ltd, Tianjin 300301, PR China

ARTICLE INFO

Article history:
Received 6 January 2010
Received in revised form 3 April 2010
Accepted 25 April 2010
Available online 5 May 2010

Keywords:
Stability
First-principles calculations
Heat capacity
Elastic constants
Hardness

ABSTRACT

The ground state properties of W–C binary compounds (h-WC, c-WC, α-W_2C, β-W_2C, γ-W_2C, ε-W_2C) are studied in this paper by using first-principles calculations. Formation enthalpy and cohesive energy for each phase are calculated. The calculated elastic constants satisfy the Born–Huang's stability criterion, indicating all studied compounds are mechanically stable. All W–C compounds studied in this paper exhibit larger bulk modulus values than many other binary types of carbide such as Fe_3C, Cr_7C_3, Cr_3C, and TiC. Using a theoretical method based on the works of Šimůnek, the hardness of the crystal is estimated. The electronic structures of these compounds are calculated and discussed. Stoner's polarization theory for itinerant magnetism is applied to explain the observed paramagnetic behavior of the compounds. Moreover, the heat capacity is also calculated for each compound based on the knowledge of the elasticity and Debye temperature.

1. Introduction

In recent decades the transition metal carbides are extensively investigated both by theoretical calculations and by experimental methods; because many of them exhibit outstanding mechanical properties and chemical stability, for instance they are very hard compounds and have high melting point, high thermal conductivity, etc. One of the most important compounds is the tungsten carbides: hexagonal and cubic mono-carbides WC, and four polymorphs (α, β, γ, ε) of semi-carbide W_2C. The properties of thermal stability and high elastic modulus determine the usage of W–C compounds in the production of wear resistant hard alloys, which form the basis of the metal cutting instruments, for example, the cemented carbide [1–4] and high-speed steel [5–7].

In all bulk W–C binary compounds, the investigations of hexagonal WC (h-WC) have been performed extensively, including the properties of bulk structures [8–10], the surfaces ((0 0 0 1) [11,12], (1 0 $\bar{1}$ 0) [13] and (1 1 $\bar{2}$ 0) [13], etc.) and the different interfaces (Al/WC [10], Fe/WC [14]). Liu et al. [8] investigated the structural and electronic properties of h-WC by performing a pseudopotential total-energy calculation. The obtained bulk modulus was 413 GPa which lies in the range of the measured values (329–577 GPa). They also found that the Fermi level locates in a deep minimum of the DOS, and the strong W–C bonds play an important role in the stability of WC. Zhukov and Gubanov [9] confirmed the extraordinary high values of bulk modulus (655 GPa) and Debye temperature (648 K) of h-WC which explain in part the superior properties of WC as a cutting material. In addition to the hcp phase, WC also exists in the NaCl-type structure (c-WC). This is a high temperature phase and can be stabilized at room temperature by a rapid quenching process applied to the liquid state [15]. The c-WC is found to be superconducting with a transition temperature of 10.0 K [16], and the h-WC is more stable than the c-WC. The electronic band structure and density of states show that the instability of NaCl-type structure is due to the occupation of anti-bonding states [17]. While less information is available for the electronic structure, stability and mechanical property of W_2C polymorphs. Until recently, Kurlov and Gusev [18] summarized the phase equilibrium in the W–C binary system and the crystal structures of all W–C carbides, who pointed out that the hardness of WC decreases slightly with increasing temperature from 300 to 1200–1300 K. Suetin et al. [19,20] reported that all W–C phases depending on their thermodynamic stability have the following sequence: h-WC > ε-W_2C > β-W_2C > γ-W_2C > α-W_2C > c-WC. Meanwhile, the abrasive resistance of WC/W_2C–(Co, Ni) alloys, the properties of cermets coatings and the WC/Metal matrix composites were investigated by other articles [21–23]. In this paper, our main interests are to study the chemical stability, electronic structures, mechanical properties (especially elastic modulus and hardness), and heat capacity of all W–C binary compounds.

* Corresponding authors at: School of Materials Science and Engineering, Xi'an Jiaotong University, 28 Xianning West Road, Xi'an, Shaanxi Province 710049, PR China. Tel.: +86 29 82665479; fax: +86 29 82665479.
E-mail addresses: yefeili@126.com (Y. Li), ymgao@mail.xjtu.edu.cn (Y. Gao).

0925-8388/$ – see front matter © 2010 Elsevier B.V. All rights reserved.
doi:10.1016/j.jallcom.2010.04.184

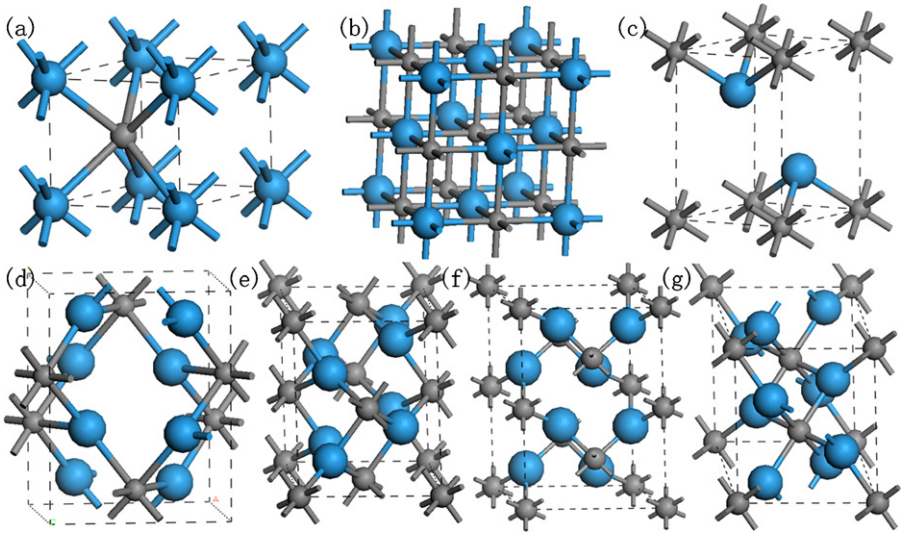

Fig. 1. Crystal structures calculated for (a) h-WC, (b) c-WC, (c) α-W_2C, (d) β-W_2C, (e) γ-W_2C_1, (f) γ-W_2C_2 and (g) ε-W_2C compounds, respectively. The small gray ball represents C atoms; the large blue ball refers to W atoms. (For interpretation of the references to color in this figure legend, the reader is referred to the web version of the article.).

2. Methods and details

Fig. 1 shows the crystal structures of W–C binary compounds. The details of the crystal structures of all W–C compounds can be found in the articles [18–20]. It is worth mentioning that in unit cell of γ-W_2C, two tungsten atoms occupy the *2c* positions and one carbon atom is randomly distributed between positions *2a* with coordinates (0 0 0) and (0 0 1/2); In another words, the carbon atoms randomly occupy one-half of all octahedral interstices in the tungsten sublattice [18]. Therefore, in the papers [19,20], Suetin considered the structure of γ-W_2C as the uniform alternation of vacancies and carbon atoms along [0 0 1] crystal direction by using supercell method. Thus, in the present paper, we also used supercell method and allowed the uniform distribution of vacancies and carbon atoms along [0 0 1], [0 1 0] and [1 0 0] crystal directions. As a result, there are two crystal structures for γ-W_2C, namely γ-W_2C_1 ([0 0 1] crystal direction) and γ-W_2C_2 ([0 1 0] or [1 0 0] crystal direction), because the symmetries of γ-W_2C along [0 1 0] and [1 0 0] are same.

All calculations in this work were performed by first-principles calculation method based on density functional theory (DFT), as implemented in CASTEP code [24–26]. The ultra-soft pseudo potentials were employed to represent the interactions between ionic core and valence electrons. For W and C, the valence electrons considered are $5s^25p^65d^46s^2$, $2s^22p^2$, respectively. In CASTEP code, the fully separable Kleinman–Bylander ultra-soft pseudopotentials were used and the relativistic effects for valence shells of heavy transition atoms were included using a scalar relativistic kinetic energy operator for Schrödinger like equation. Generalized gradient approximation (GGA) of PBE approach was used for exchange-correlation energy calculations [27]. A kinetic energy cut-off value of 400 eV was used for plane wave expansions. The total-energy integrations were evaluated in the first irreducible Brillouin zone with Monkhorst–Pack scheme at special *k* points [28], for example 10 × 10 × 10 and 15 × 15 × 15 for electronic optimizations and elastic constants calculations, respectively. In order to investigate the chemical stability of these compounds at given *P*/*T* conditions, the cohesive energy and formation enthalpy were calculated using

$$E_{coh}(WC) = E_{tot}(WC) - E_{iso}(W) - E_{iso}(C) \quad (1)$$

$$\Delta_r H(WC) = E_{coh}(WC) - E_{coh}(W) - E_{coh}(C) \quad (2)$$

$$E_{coh}(W_2C) = E_{tot}(W_2C) - 2E_{iso}(W) - E_{iso}(C) \quad (3)$$

$$\Delta_r H(W_2C) = E_{coh}(W_2C) - 2E_{coh}(W) - E_{coh}(C) \quad (4)$$

where E_{coh}(X) and $\Delta_r H$ (X) is the cohesive energy, formation enthalpy of X phase, respectively; E_{tot}(X) is the total-energy of X material and E_{iso}(X) denotes the total-energy of a single X atom. The influence of hydrostatic pressure on the formation enthalpy was investigated in this paper, the crystal structures were fully optimized at each pressure and then the total cell energy was obtained. For computational convenience, the calculations were performed at $T = 0$ K, thus, the formation enthalpy equals to the free energy, which reflects the thermodynamical stability.

3. Results and discussions

3.1. Stability

In Table 1, we depict the calculated cell parameters, cohesive energy and formation enthalpy of all modifications of WC and W_2C compounds. Generally speaking, the calculated cell constants

Table 1
The calculated cell parameters (*a*, *b*, *c*, in Å; *ρ* in g/cm³; V_{cell} in Å³), atomic positions for W and C atoms (fractional coordinates), cohesive energy (eV/atom), formation enthalpy (eV/atom) of W–C carbides (including h-, c-WC and α-, β-, γ-, ε-W_2C polymorphs).

Phase	h-WC	c-WC	α-W_2C	β-W_2C	γ-W_2C_1	γ-W_2C_2	ε-W_2C
Space group	$P\bar{6}m2$	$Fm\bar{3}m$	$P\bar{3}m1$	*Pbcn*	P_1[1]	P_1[1]	$P\bar{3}1m$
a	2.906 (2.906[a,b])	4.351 (4.265[a])	3.043 (3.001[a])	4.725 (4.728 [a,c])	3.043 (3.002[a], 2.992[d])	3.029 (3.002[a])	5.211 (5.184[a])
b				6.057 (6.009 [a,c])	6.087	6.090	
c	2.825 (2.837[a,b])		4.655 (4.728[a])	5.195 (5.193[a,c])	4.707 (4.75[a], 4.725[d])	4.707 (4.75[a])	4.752 (4.721[a])
V_{cell}	20.6558	82.3748	37.3251	148.6584	150.649	150.655	111.7365
ρ	15.74	15.79	16.89	16.97	16.742	16.741	16.93
W	(0 0 0)	(0 0 0)	(0.3333 0.6667 0.25)	(0.25 0.125 0.083)	(0.6667 0.3333 0.25)	(0.6667 0.3333 0.25)	(0.3333 0 0.25)
C	(0.3333 0.6667 0.5)	(0.5 0.5 0.5)	(0 0 0)	(0 0.375 0.25)	(0 0 0)	(0 0 0)	(0 0 0) (0.3333 0.6667 0.5)
E_{coh}	−10.64	−10.19	−10.79	−10.87	−10.89	−10.89	−10.86
$\Delta_r H$	−0.106 (−0.170[e])	0.341 (0.281[e])	0.065 (0.063[e])	−0.018 (−0.007[e])	−0.029 (0.006[e])	−0.030	−0.003 (−0.013[e])

[a] Experimental data summarized in Ref. [18].
[b] Inorganic Crystal Structure Database (ICSD) #43380.
[c] ICSD #43017.
[d] ICSD #77567.
[e] FP-LMTO method in Ref. [20].
[1] γ-W_2C has space group $P6_3/mmc$, the supercell was used and the corresponding space group is P_1.

of all W–C compounds are in good agreement with experimental results. The average deviation of our results to experimental results for lattice constants is 2%. Because GGA was used in our works; one could expect that it may overestimate the cell constants for some W–C binary compounds. Two thermodynamic parameters are used to determine the relative stability of all W–C phases. They are the cohesive energy and formation enthalpy. As defined in Eqs. (1)–(4), the smaller the negative values of these two parameters, the more stable the compound. The cohesive energies of all these carbides have negative values, but their formation enthalpies are quite different from each other. It is obvious that h-WC, β-W_2C, γ-W_2C_1, γ-W_2C_2 and ε-W_2C are stable structures, which show negative enthalpy value of −0.106, −0.018, −0.029, −0.03 and −0.003 eV/atom., respectively. However, the formation enthalpy of c-WC and α-W_2C is positive, i.e. these species are meta- or un-stable, The stability sequence of six W–C phases forms the following order: h-WC > γ-W_2C_2 ≈ γ-W_2C_1 > β-W_2C > ε-W_2C > α-W_2C > c-WC, which differs to the results obtained by Suetin et al. [19,20]. It is probably caused by the different calculation methods such as potential functions mentioned above. Among four W_2C polymorphs, two modified γ-W_2C crystals are more stable, and the calculated cohesive energy and formation enthalpy of them are smaller than other three W_2C crystals. The results may indicate that the randomly distributed carbon vacancies at (0 0 0 1) crystal plane do not show superior orientations. In addition, in the literature [18], the authors reported that the temperature induced consecutive phase transformations of W_2C polymorphs occur with the following sequences

$$\gamma - W_2C \rightleftharpoons \beta - W_2C \quad (5)$$

$$\beta - W_2C \rightleftharpoons \varepsilon - W_2C \quad (6)$$

$$c - WC \rightleftharpoons h - WC \quad (7)$$

The polymorphic transformation temperatures are ~2750, ~2728, and ~3008 K, respectively, which were determined by using the high temperature differential thermal analysis involved in a highly sensitive optical system. Note that the Eq. (5) is a disorder–order transformation. These transformation sequences are in agreement with the formation enthalpy differences as can be seen from Table 1. The large enthalpy difference between low and high temperature phases may be responsible for high transformation temperature.

On the other hand, the external pressure induced phase transformations are frequently observed in many oxides, carbides and borides of transition metals and which have been extensively studied. However, the data on the phase stability for the polymorphic modifications of the W–C binary compounds caused by hydrostatic pressure are absent. Fig. 2 presents the formation enthalpy curves as a function of hydrostatic pressures for all W–C structures. It is clear that the calculations for h- and c-WC polymorphs correctly predict the stability of h-WC is better than that of c-WC at high pressure, and the phase transformations are not driven by pressure, because the enthalpy curves almost parallel or departure from each other. For W_2C polymorphs, the γ-W_2C phase is stabilized up to ~80 GPa and then transforms to β-W_2C with the *Pbcn* structure, and β-W_2C is found to be the most stable phase among W_2C polymorphs at the pressure range of 80–200 GPa. Another pressure induced phase transformation occurs at 150 GPa between γ-W_2C and ε-W_2C. Calculating the phonon spectrum of these W_2C polymorphs as a function of hydrostatic pressure can provide more details about the phase transformations which are not carried out in present paper. Comparing the enthalpy curves of WC in Fig. 2(a) to those of W_2C in Fig. 2(b), we conclude that the chemical stability of WC polymorphs is less sensitive to the hydrostatic pressure than that of W_2C compounds. Thus h-WC will have high mechanical stability at high pressures and is suitable to be used as reinforced phase in composites.

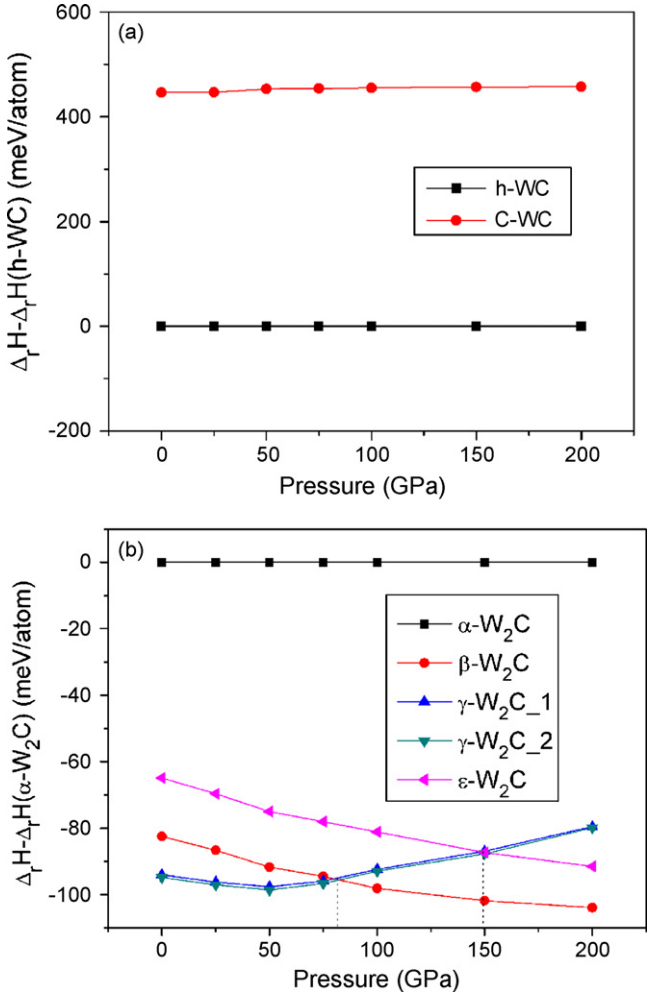

Fig. 2. Calculated formation enthalpy values vs hydrostatic pressures for the (a) h- and c-WC polymorphs and (b) α-, β-, γ-, ε-W_2C polymorphs. For WC polymorphs, the $P\bar{6}m2$ structure is taken as reference; for W_2C phases, enthalpies are shown with respect to the $P\bar{3}m1$ structure.

3.2. Electronic structures

In this part, three parameters are used to indicate the electronic structures and chemical bonding characteristics of all W–C phases, which are density of states (DOS), electron density distribution map and population analysis. For h-WC, as shown in Fig. 3a, the Fermi level is situated close to a minimum of the DOS qualitatively indicating its stability nature, while for c-WC, the Fermi level lies at the local maximum of DOS, destabilizing the NaCl-like structure of WC. In contrast to WC crystals, all W_2C polymorphs have relatively large values of DOS at Fermi level, which reproduce the results obtained by Suetin et al. [19,20], indicating they are less stable than h-WC.

The calculated total electron density distribution maps of these compounds are shown in Fig. 4. In all figures, even in the interstitial regions the electron density values are greatly larger than zero, which clearly indicate the metallic nature of W–C compounds. The elongated contours along W–C bond axis can be ascribed to the covalent interactions; this provides an evidence to explain the covalent bonds caused by hybridization of C-2p and W-5d orbitals [9,10,19]. As was already mentioned, the calculated DOS of h-WC has a minimum near the Fermi level which is a reflection of the splitting of bonding and anti-bonding states created by the

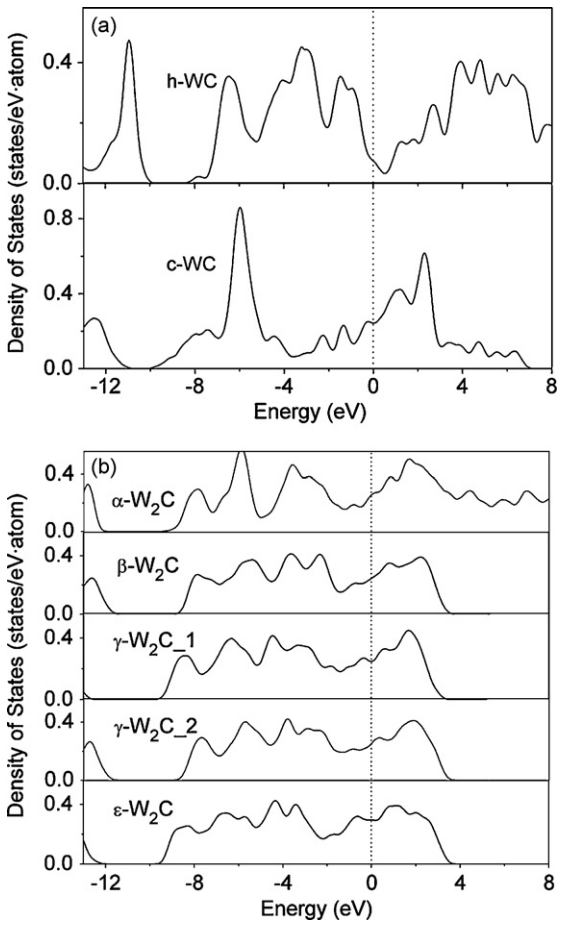

Fig. 3. Total density of states of (a) WC and (b) W_2C polymorphs. Dashed lines represent the Fermi level.

hybridization of 2p and 5d orbitals. The bonding states are mainly consisted of 2p bands of C and the anti-bonding states above the Fermi level are 5d bands of W. When W/C = 1, for instance h-WC, the bonding states below the Fermi level are fully occupied and the anti-bonding states are unoccupied. As a result, h-WC has the highest stability among W–C binary compounds. W_2C represents the W rich condition, implying that the some anti-bonding states are also occupied. The calculated DOS curves for W–C binary compounds obviously have such features. There is a local minimum in the calculated DOS of γ-W_2C_1 and which is absent in γ-W_2C_2. The calculated formation enthalpy for γ-W_2C_1 is comparable to γ-W_2C_2.

Magnetism is rarely observed in compounds of 4d and 5d transition metals, and they are paramagnetic compounds. Stoner's polarization theory is prevalently used to explain the local magnetic moments of metal atoms for 3d, 4d and 5d transition metals and their compounds, because the DOS of them always has strong metallic character. Itinerant magnetism can be observed when Stoner's condition is satisfied, that is $N_f I > 1$. Here, N_f is the density of d states only at the Fermi level in unit states/eV·atom and I characterizes the internal exchange parameter of d electrons (unit in eV/atom), I is independent of the crystal structures. It is previously suggested that for 3d, 4d and 5d transition metals, the I value is 0.9, 0.65 and 0.3, respectively [29–32]. As a result, the critical DOS values for 5d transition metals and the corresponding compounds are 3 states/eV·atom. As can be seen from Table 2, no W–C binary compound could fulfil such a condition, indicating that all of WC and W_2C polymorphs are paramagnetic compounds. Furthermore, we also calculated Pauli paramagnetic susceptibilities for W–C binary compounds using $\chi = \mu_B^2 D_F$, where χ is Pauli paramagnetic susceptibility, μ_B is Bohr magnetic moment and D_f represents the total density of states at Fermi level, and the results are listed in Table 2 as well. The results for W_2C polymorphs are very close to ref. [19].

Population analysis results can provide more insightful information on chemical bonding, which are listed in Table 3. Mulliken method is applied for the overlap population and the charge calculations. We used Eqs. (8) and (9) to calculate the average bond length and the average overlap population:

$$\overline{L}(\mathrm{AB}) = \frac{\sum L_i N_i}{\sum N_i} \tag{8}$$

$$\overline{n}(\mathrm{AB}) = \frac{\sum n_i N_i}{\sum N_i} \tag{9}$$

Here, $\overline{L}$(AB) and $\overline{n}$(AB) represent the average bond length and the mean bond population, respectively; N_i is the total number of i bond in the cell and L_i is the bond length of i type.

First of all, we want to list the electronegativity value of W and C atoms in Pauling scale: 2.55 (C), 1.7 (W). As shown in Table 3, it is clearly indicated that C carries the negative charges for all of the

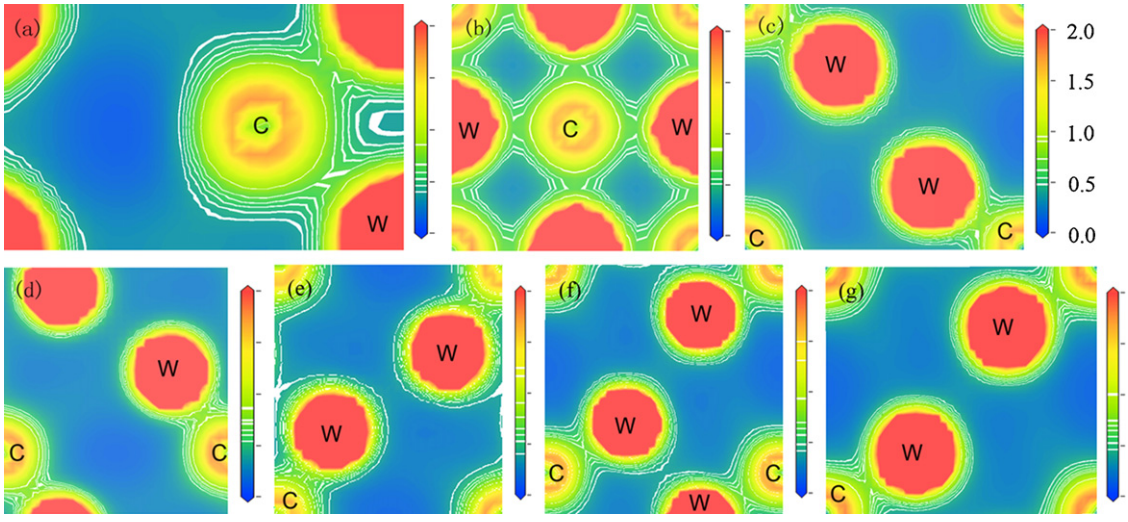

Fig. 4. Total electron density distribution through (1 1 0), (0 0 1), (1 1 0), (0 1 0), (1 1 1), (1 1 1) and (1 −1 0) slice intersecting both W and C atoms for (a) h-WC, (b) c-WC, (c) α-W_2C, (d) β-W_2C, (e) γ-W_2C_1, (f) γ-W_2C_2 and (g) ε-W_2C compounds, respectively. The electron density contours were plotted from 0 to 2.0 e/Å^3.

Table 2
The calculated Stoner's parameters ($N_f I$), Pauli paramagnetic susceptibilities (χ, 10^{-4} emu/mol) and the metallicity parameter for W–C binary compounds; D_f is the total density of states at the Fermi level (states/(eV·atom)), and N_f is the DOS value at the Fermi level for d state only (states/(eV·atom)).

Species	h-WC	c-WC	α-W_2C	β-W_2C	γ-W_2C_1	γ-W_2C_2	ε-W_2C
D_f	0.075 (0.115[a], 0.119[b])	0.243 (0.134[b], 0.157[c])	0.260 (0.231[d])	0.246 (0.245[d])	0.270 (0.275[d])	0.255	0.290 (0.297[d])
N_f	0.122 (0.099[d])	0.369 (0.682[d])	0.342 (0.378[d])	0.322 (0.386[d])	0.244 (0.423[d])	0.329	0.372 (0.463[d])
N_f·I	0.037	0.111	0.103	0.097	0.073	0.099	0.112
χ	0.05 (0.07[d])	0.157 (0.43[d])	0.252 (0.224[d])	0.239 (0.238[d])	0.262 (0.267[d])	0.247	0.281 (0.289[d])
f_m	0.009	0.110	0.031	0.119	0.132	0.124	0.105

(a–c) The data are obtained using the linear muffin-tin orbital (LMTO) method in Refs. [17,34,35], which differ from our results using partial wave analysis (PWA) method. (d) FLAPW-GGA method in Ref. [19,20].

W–C compounds, and the value varies from −0.6 (h-WC) to −0.71 (ε-W_2C). The largest positive charges are carried by W atoms of c-WC. One can propose two possible electron transfer paths intra or inter the C and W atoms. The one refers to p-d hybridized covalent bonding between C and W, and the other one is induced by the metallic bonding among W atoms. In the former case, the electrons are transferred from W to C, and can be designated as 6s (W) to 2p (C) for all W–C compounds. Besides, for β- and ε-W_2C, W–W bonds show positive overlap populations, implying a metallic bonding character between tungsten atoms. From Fig. 4 it can be seen that the metallic W–W bond is so strong that it cannot be simply neglected. In fact, Stadler et al. [33] studied the electronic structures of W_2B both by using experimental methods and DFT calculations, they found that a shallow spitting of d bands, and which implies strong d–d metallic bonding between W atoms; for α-W_2C, W–W bonds have negative overlap populations, which indicates anti-bond states or strong electrostatic repulsion among tungsten atoms. The similar negative bond populations can also be seen in C–C bonds for β- and γ-W_2C. Thus, the covalent interactions for all W–C compounds are mainly determined by W–C bonds. Otherwise, the metallicity of the tungsten carbides is ascribed to W–W bonds. The metallicity of the compound is estimated by

$$f_m = \frac{n_m}{n_e} = \frac{k_B T D_f}{n_e} = \frac{0.026 D_f}{n_e} \quad (10)$$

where D_f is the DOS value at the Fermi level in unit states/eV·cell, and T is the temperature; n_m and n_e are the thermal excited electrons and valence electron density of the cell, respectively; k_B is the Boltzmann constant. n_e is calculated by $n_e = N/V_{cell}$, N is the total number of valence electrons and V_{cell} is the cell volume. The related parameters and calculated results are shown in Table 2, from which we can observed that f_m increases in the following sequence: h-

Table 3
Mulliken population analysis results of all W–C compounds: $\overline{n}$ is average population, $\overline{L}$ is average bonding length. Note that total charges of s and p orbitals of W are calculated as 5s + 6s and 5p + 6p, respectively.

Polymorph	Species (Ion)	s	p	d	Total electrons	Charges
h-WC	C	1.37	3.23	0	4.6	−0.6
	W	2.46[a]	6.51[b]	4.43	13.4	0.6
c-WC	C (1–4)	1.39	3.3	0	4.69	−0.69
	W (1–4)	2.35	6.44	4.52	13.31	0.69
α-W_2C	C	1.39	3.26	0	4.65	−0.65
	W (1–2)	2.43	6.66	4.58	13.67	0.33
β-W_2C	C (1–4)	1.38	3.32	0	4.69	−0.69
	W (1–8)	2.41	6.66	4.59	13.65	0.35
γ-W_2C_1	C (1–4)	1.38	3.31		4.69	−0.69
	W (1–8)	2.40	6.67	4.58	13.65	0.35
γ-W_2C_2	C (1–4)	1.38	3.31		4.69	−0.69
	W (1–8)	2.40	6.67	4.58	13.65	0.35
ε-W_2C	C (1)	1.37	3.34	0	4.71	−0.71
	C (2–3)	1.38	3.31	0	4.69	−0.69
	W (1–6)	2.41	6.66	4.58	13.65	0.35

Polymorph	Bond	$\overline{n}$ (electrons)	$\overline{L}$ (Å)
h-WC	C–W	2.1	2.19
c-WC	C–W	0.8	2.18
α-W_2C	C–W	0.89	2.12
	W–W	−0.20	2.89
β-W_2C	C–W	0.31	2.11
	W–W	0.13	2.91
	C–C	−0.08	2.99
	WW	0.27	2.99
γ-W_2C_1	C–W	0.34	2.12
	W–W	0.23	2.91
γ-W_2C_2	C–W	0.47	2.12
	W–W	0.14	2.91
ε-W_2C	C–W	0.26	2.11
	W–W	0.16	2.96

Note: (a) 5s + 6s; (b) 5p + 6p.

Table 4
Calculated values for the independent elastic constants (C_{ij}, in GPa), bulk moduli (B, in GPa), shear moduli (G, in GPa), Young modulus (E, in GPa) and Poisson's ratio (υ) of W–C binary compounds.

Polymorph	h-WC	c-WC	α-W_2C	β-W_2C	γ-W_2C_1	γ-W_2C_2	ε-W_2C
C_{11}	711.6 (772.8[a,b], 720[c])	696.5 (706.5[a])	531.6	528.4	508.8	535.8	546.8
C_{12}	240.6 (209.9[a,b], 254[c])	215.5 (191.4[a])	144.6	255.5	196.3	178.18	194.4
C_{13}	168 (157.8[a,b], 267[c])		244.9	269.7	256.9	243.6	267
C_{14}							11.2
C_{22}				548			
C_{23}				188.1			
C_{33}	977.5 (960.6[a,b], 972[c])		549.6	565.8	489.8	526.4	509.6
C_{44}	305.1 (302.2[a,b], 328[c])	122 (151.6[a])	167	160.7	206.7	216.9	212
C_{55}				187.1			
C_{66}	235.5 (256.4[a,b])	122 (151.6[a])	193.5	221.3	167.7	174.5	176.2
B_V	394.87 (384.2[a])	375.86 (363.1[a])	320.18	340.99	327.9	328.4	339.98
G_V	290.76 (297.5[a])	169.41 (194.0 [a])	170.72	175.74	162.8	177.6	178.36
B_R	391.16 (380.7[a])	375.88 (363.1[a])	316.29	340.21	327.2	327.4	339.59
G_R	281.58 (291.7[a])	151.96 (181.5[a])	166.97	169.42	154.1	171.9	169.32
B (B_{VRH})	393 (382.4[a], 391[d], 442.83[e], 421[f])	375.9 (363.1[a])	318.2	340.6	327.5	327.9	339.8
G (G_{VRH})	286.2 (294.6[a], 269[f])	160.7 (187.7[a])	168.8	172.6	158.4	174.7	173.8
B/G	1.37 (1.29[a])	2.34 (1.93[a])	1.89	1.97	2.07	1.88	1.96
E	690.9 (703.2[a], 706.75[e])	422.7 (480.4[a])	430.3	443.0	409.2	445.1	445.5
ν	0.207 (0.194[a])	0.313 (0.279[a])	0.275	0.283	0.292	0.274	0.282
C_{11}/C_{33}	0.72 (0.80[a])	1	0.98	0.93	1.04	1.02	1.07
C_{12}/C_{13}	1.24 (1.33[a])	1	0.60	0.94	0.76	0.73	0.72
C_{44}/C_{66}	1.29 (1.18[a])	1	0.86	0.72	1.23	1.16	1.20

[a] Calculated by FLAPW with GGA scheme in Ref. [41].
[b] FLAPW-GGA calculation results in Ref. [42].
[c] Experimental results measured by the high-frequency ultrasonic method in Ref. [43].
[d] FLAPW-GGA calculation results in Ref. [44].
[e] Calculation data from Ref. [45], at the temperature of 50 K.
[f] Ref. [46].

WC < α-W_2C < ε-W_2C < c-WC < β-W_2C < γ-W_2C_2 < γ-W_2C_1. Thus, the maximal and minimal "metallicity" correspond to the γ-W_2C and the h-WC, respectively.

Based on the above discussions, the bonding behaviors of W–C compounds are the combinations of metallic, covalent and ionic bonds, which lead to the high melting point, high hardness, and good electric conductivity. In fact, transition metals form many sorts of carbides, such as TiC, VC, Fe_3C, and Cr_7C_3, in which the mixture bonding states are always observed [36,37].

3.3. Mechanical properties

The mechanical performances of the studied W–C system compounds play an important role for the application as wear resistance material. The elastic stiffness determines the response of a crystal to an imposed strain [38]. It is essential to investigate the elastic stiffness to understand the mechanical properties of W–C compounds. Therefore, a stress–strain approach, based on the generalized Hooke's law, was employed to calculate elastic constants in this work. The calculated independent elastic stiffness constants (C_{ij}) are illustrated in Table 4. According to Born–Huang's lattice dynamical theory, the mechanical stability criterions can be expressed as [39,40]:

Hexagonal system (for h-WC, γ-W_2C_1 and γ-W_2C_2):

$$C_{11} > 0,\ \ C_{44} > 0,\ \ (C_{11} - C_{12}) > 0,\ \ (C_{11} + C_{12})C_{33} > 2C_{13}^2 \quad (11)$$

Cubic system (for c-WC):

$$C_{11} > 0,\ \ C_{44} > 0,\ \ C_{11} - C_{12} > 0,\ \ C_{11} + 2C_{12} > 0 \quad (12)$$

Trigonal system (for α-W_2C and ε-W_2C):

$$C_{11} > \left|C_{12}\right|,\quad (C_{11} + C_{12})C_{33} > 2C_{13}^2,\quad (C_{11} - C_{12})C_{44} - 2C_{14}^2 > 0 \quad (13)$$

Orthorhombic system (for β-W_2C):

$$C_{11} + C_{12} + C_{33} + 2C_{12} + 2C_{13} + 2C_{23} > 0,\quad C_{11} + C_{22} > 2C_{12},\ \ C_{22} + C_{33} > 2C_{23},\ \ C_{11} + C_{33} > 2C_{13},\ \ C_{ii} > 0\ \ (i = 1 - 6) \quad (14)$$

It is worth noting that the crystal structures of γ-W_2C_1 and γ-W_2C_2 should have hexagonal symmetry (with space groups of $P6_3/mmc$), since the supercell method is carried out to deal with γ-W_2C (with space group P_1). Therefore, only the independent elastic constants identical to hexagonal cell are listed in Table 4 for two γ-W_2C modifications. As shown in Table 4, the calculated elastic constants of each W–C compound satisfy the above corresponding criterion, respectively, indicating that all of W–C compounds are mechanically stable. For W–C system compounds, the calculated C_{11} and C_{33} are very large among elastic constants which indicates that they are very incompressible under uniaxial stress along x (ε_{11}) or z (ε_{33}) axis. Besides, for two WC polymorphs, the obtained C_{11} and C_{33} of h-WC are larger than c-WC, indicating the strong directional bonding in h-WC crystal along [1 0 0] direction. Among all W–C binary compounds, h-WC has the largest C_{11} value as 711.6 GPa. The calculated elastic constants of h-WC are in agreement with other references. For c-WC, the agreement with FLAPW results varies for different elastic constants. The largest deviation between them is 30 GPa. C_{44} indicates the resistances of the crystal with respect to the shear strain at (1 0 0) plane, and which is closely related to the shear modulus. From Table 4, one can see that h-WC has the largest C_{44} value for all studied W–C binary compounds and γ-W_2C_2 has the largest C_{44} value among W_2C polymorphs. We also calculated C_{11}/C_{33}, C_{12}/C_{13} and C_{44}/C_{66} values in order to illustrate the elastic anisotropy for each W–C compound. Due to the symmetric restrictions on tensor elements, the obtained values are unity for c-WC. However, for other W–C binary compounds, the calculated ratios deviate from the unity, showing the mechanical anisotropy. The bulk modulus (B), shear modulus (G), Young's modulus (E) and Poisson's ratio (υ) for polycrystalline crystal can be obtained from independent single crystal elastic constants. Usually, the polycrystalline modulus is estimated within Voigt and Reuss methods [38], in which the former method is based on assumption of uniform strain throughout a polycrystal, which is given by:

$$B_V = \frac{1}{9}(C_{11} + C_{22} + C_{33}) + \frac{2}{9}(C_{12} + C_{23} + C_{13}) \quad (15)$$

$$G_V = \frac{1}{15}(C_{11} + C_{22} + C_{33}) - \frac{1}{15}(C_{12} + C_{23} + C_{13}) + \frac{1}{5}(C_{44} + C_{55} + C_{66}) \quad (16)$$

The latter method assumes a uniform stress and gives B and G as functions of the elastic compliance constants S_{ij}, which is the inverse matrix of C_{ij}.

$$\frac{1}{B_R} = (S_{11} + S_{22} + S_{33}) + 2(S_{12} + S_{23} + S_{13}) \quad (17)$$

$$\frac{1}{G_R} = \frac{4}{15}(S_{11} + S_{22} + S_{33}) - \frac{4}{15}(S_{12} + S_{23} + S_{13}) + \frac{1}{5}(S_{44} + S_{55} + S_{66}) \quad (18)$$

where the subscripts V and R indicate the Voigt and Reuss averages. The arithmetic average of Voigt and Reuss bounds is termed as the Voigt–Reuss–Hill approximations, and it is considered as the best estimation of the theoretical polycrystalline elastic modulus. In addition, the polycrystalline Young's modulus and Poisson's ratio can be calculated from the values of elastic modulus as follows [40]:

$$E = \frac{9BG}{3B + G} \quad (19)$$

$$\upsilon = \frac{3B - 2G}{2(3B + G)} \quad (20)$$

Bulk modulus reflects the compressibility of the solid under hydrostatic pressure. The bulk modulus of W–C system compounds are 393, 375.9, 318.2, 340.6, 327.5, 327.9 and 339.8 GPa for h-WC, c-WC, α-W_2C, β-W_2C, γ-W_2C_1, γ-W_2C_2 and ε-W_2C phases, respectively, which exhibit larger values than the common carbides such as Fe_3C (276 [47], 226.8 [48]), Cr_7C_3 (311.7 [37], 309 [49]), Cr_3C (298.24 [37]), and TiC (249 [50], 242 [51]), but smaller than that of diamond (436.8 [52]). The Poisson's ratios (υ) of there compounds range from 0.207 (h-WC) to 0.313 (c-WC), which is near 0.3 and clearly illustrates the strong metallic character of W–C compounds. The largest discrepancy of υ from 0.3 is observed for h-WC mainly caused by the ionic nature of crystal (typically, for ionic crystal, the value is near 0.25). Then the shear modulus is calculated and the values are 286.2, 160.7, 158.8, 172.6, 158.4, 174.7 and 173.8 GPa for h-, c-WC and all kinds of W_2C polymorphs. The ratio of B/G is frequently used to indicate the ductility of the compound, it is supposed that for the brittle compound, B/G is smaller than 1.75 (for diamond $B/G = 0.8$) and for metallic compound B/G is greater than 1.75 (for Al $B/G = 2.74$). In our case, the calculated results clearly imply that h-WC is more brittle than other W–C compounds, since the Fermi level is situated close to a minimum of the DOS and the metallicity in h-WC is less remarkable than other W–C phases. Finally, the Debye temperature for each compound is calculated based on the knowledge of elastic constants and will be discussed in Section 3.4.

Table 5
Equation of States fitted bulk modulus (B, in GPa) and its pressure derivative of W–C carbides and several other hard compounds.

Species	h-WC	c-WC	α-W_2C	β-W_2C	γ-W_2C_1	γ-W_2C_2	ε-W_2C	Cr_7C_3	OsB_2	OsO_2	diamond	Fe_3C	Fe_2B	TiB_2
B_0	400.9	374.4	343.3	353.5	343.9	343	341.9	311.7[a]	329.8[b]	282.3[b]	436.8[b]	259.2[a]	331[a]	213[c]
B_0'	4.06	4.33	4.32	3.11	3.62	4.78	5.5	4.26[a]	4.17[b]	4.52[b]	3.30[b]	4.25[a]	4.4[a]	2.1[c]

[a] Ref. [35].
[b] Ref. [52].
[c] Ref. [53].

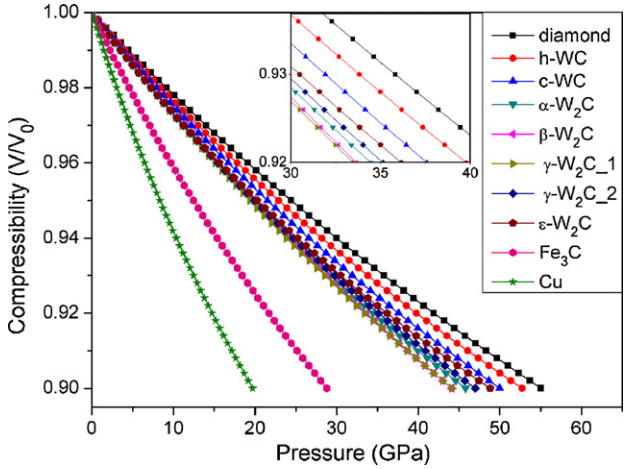

Fig. 5. The compressibility curves of W–C binary compounds; for comparisons, the profiles of Fe_3C, Cu and diamond are also shown.

In this part, we would like to discuss the compressibility of all W–C compounds. We fitted the total-energy (E) as function of cell volume (V) by using well-known Birch–Murnaghan equation of state (Eq. (21)).

$$\begin{cases} E(V) = \dfrac{B_0 V_0}{B_0'}\left[\dfrac{1}{B_0'-1}\left(\dfrac{V}{V_o}\right)^{(1-B_0')} + \dfrac{V}{V_0} + \dfrac{B_0'}{1-B_0'}\right] + E_0 \\ P(V) = \dfrac{B_0}{B_0'}\left[\left(\dfrac{V_0}{V}\right)^{(B_0')} - 1\right] \end{cases} \quad (21)$$

Here, because the applied stress is up to 200 GPa, and the crystal cells have been compressed into only 3/4 of the equilibrium cell volumes for all W–C compounds, which may cause large errors because of the plastic deformation. Thus we fitted the E–V curves again by changing the cell volumes at the range of −10 to 10%, from which we obtained several mechanical parameters as shown in Table 5. The obtained bulk moduli of all W–C compounds are close to the results in Table 4, which indicate the reliability of our calculations. Fig. 5 shows the compressibility of W–C compounds. For comparisons, the results for Cu and diamond are also shown. The hardest material always situated in the upper part of the figure, because it is hard to compress, the relationship between the hardness and bulk modulus is still unclear, but hard materials usually favor large bulk modulus. In summary, W–C binary compounds are more incompressible than Cr_7C_3, Fe_3C, Cr_3C, TiC, etc.

The hardness of a material always plays an important role in its applications, especially using as an abrasive resistant phase [54]. Thus it is necessary to investigate the hardness of W–C carbides because of its foundation status in the wear resistance materials. According to Šimůnek's theory [55,56], the theoretical hardness of single crystal can be calculated within the following forms.

$$H = \frac{C}{\Omega} n \left[\prod_{i,j=1}^{n} b_{ij} s_{ij}\right]^{1/n} e^{-\sigma f_e} \quad (22)$$

$$f_e = 1 - \left[k \frac{\left(\prod_{i=1}^{k} e_i\right)^{1/k}}{\sum_{i=1}^{k} e_i}\right]^2 \quad (23)$$

$$s_{ij} = \frac{\sqrt{e_i e_j}}{n_i n_j d_{ij}} \quad (24)$$

where the reference energy $e_i = Z_i/R_i$, Z_i is the valence electron number of the atom i, and R_i is the radius of the sphere in which Z_i electrons are contained, because the change of e_i values for same atom in difference compounds are small [55], so in this work, we assumed that e_C and e_W are 3.764 and 3.971, respectively; n_i and n_j are coordination numbers of atoms i and j, respectively; d_{ij} is the interatomic distance between atoms i and j; k corresponds to the number of different atoms in the system; s_{ij} is the strength of the individual bond between atoms i and j; b_{ij} is the individual bond in the unit cell; the constants $C = 1550$ and $\sigma = 4$ [55] are used throughout this work. Using Eqs. (22)–(24) we have calculated the hardness of all W–C binary compounds as shown in Table 6.

The obtained hardness of h-WC is in satisfactory agreement with the previous calculation by Šimůnek and Vackář [55]. It is interesting that B and G of h-WC are as high as 393 and 286.2 GPa, respectively, but its hardness is only 22 GPa (for diamond, the hardness is 95.4 GPa [55]), providing a direct evidence that it is difficult to describe hardness quantitatively only by elastic moduli of B and G. Moreover, it is noteworthy that the hardness values for h-WC and c-WC are all smaller than those of W_2C polymorphs. This is mainly

Table 6
The predicted hardness and parameters related to the hardness calculations of h-, c-WC and α-, β-, γ-, ε-W_2C polymorphs.

Phase	h-WC	c-WC	α-W_2C	β-W_2C	γ-W_2C_1	γ-W_2C_2	ε-W_2C
d_{12}	2.193(2.194[a])	2.176	2.116	2.110	2.121	2.121	2.103
n_1	6	6	6	6	6	6	6
n_2	6	6	3	3	3	3	3
b_{12}	6	24	6	24	24	24	18
s_{ij} (W–C)	0.0490	0.0494	0.1015	0.1018	0.1013	0.1013	0.1021
H (GPa)	22 (21.5[a] 30[b], 35.6[c], 26.4[d])	22.25	25.22	25.4	24.94	24.94	25.42

[a] Ref. [55].
[b] Ref. [57].
[c] Ref. [58].
[d] Ref. [59].

Table 7
Theoretically calculated thermal properties of the W–C compounds, including the longitudinal sound velocity (v_l, m/s), shear sound velocity (v_s, m/s), and average sound velocity (v_m, m/s), Debye temperature (Θ_D, K), the characteristic parameters of electron (γ, mJ/(K^2·mol)) and phonon (β, mJ/(K^4·mol)) specific heat.

Phases	v_l	v_s	v_m	Θ_D	γ	β
h-WC	7013.9376	4263.4185	4710.2989	591.32 (493[a], 621[a])	0.36 (0.79[a], 0.54[b])	0.0188 (0.0162 [a])
c-WC	6113.1636	3189.9702	3569.0106	448.49	1.14 (3.31[b], 0.74[c])	0.043
α-W_2C	5670.9486	3161.0794	3519.7311	452.34	1.83 (1.63[d])	0.0629
β-W_2C	5800.0365	3189.5874	3555.2344	457.56	1.74 (1.73[d])	0.0607
γ-W_2C_1	5672.5066	3075.9488	3432.1962	439.77	1.91 (1.94[d])	0.0684
γ-W_2C_2	5787.9692	3230.3959	3596.5487	460.83	1.80	0.0595
ε-W_2C	5810.4051	3204.1329	3570.6867	459.22	2.05 (2.1[d])	0.0601

[a] The values are derived by measuring the low-temperature heat capacities of h-WC from 1.5 to 15 K in Ref. [64].
[b] Theoretical data in Ref. [19].
[c] Ref. [17].
[d] Theoretical data in Ref. [20].

due to the small coordination numbers of W atoms for W_2C polymorphs. For all W_2C structures, W atoms are placed in the corner of an irregular tetrahedron which result in the large bond strength S_{ij}.

3.4. Heat capacity

Once known the elastic constants and electronic structures of the compound, one can calculate the Debye temperature and heat capacity at the low-temperature. Debye temperature gives some insight into the thermodynamics of material from the elastic properties; it can be used to distinguish between high- and low-temperature regions for a solid. For $T > \Theta_D$, all modes have energy of k_BT; and for $T < \Theta_D$ one expects high-frequency modes to be frozen [60]. The Θ_D can be estimated from the average sound velocity by the following equations [61,62]:

$$\Theta_D = \frac{h}{k_B}\left[\frac{3n}{4\pi}\left(\frac{N_A\rho}{M}\right)\right]^{1/3} v_m \quad (25)$$

$$v_m = \left[\frac{1}{3}\left(\frac{2}{v_s^3} + \frac{1}{v_l^3}\right)\right]^{-1/3} \quad (26)$$

$$v_l = \sqrt{\left(B + \frac{4}{3}G\right)\frac{1}{\rho}}, \quad v_s = \sqrt{G/\rho} \quad (27)$$

where Θ_D is the Debye temperature; h and k_B are the Planck and Boltzmann constant, respectively; n is the total number of atoms per formula; N_A represents the Avogadro number; M is the molecular weight per formula; v_m is the average sound velocity; v_l is the longitudinal sound velocity and v_s the shear sound velocity. The calculated results ofΘ_D, v_l and v_s are listed in Table 7, the calculated averaged elastic wave velocities of these carbides are relatively large which are around 3500 m/s. A reasonable explanation is these compounds have large B and G values. The largest Θ_D is 591.32 K for h-WC. It is known that the Θ_D can be used to characterize the strength of covalent bonds in solids. From Table 7, we can conclude that the covalent bond in h-WC is stronger than the other carbides. Besides, the sequence ofΘ_D for W–C compounds is: h-WC > γ-W_2C_2 ≈ ε-W_2C ≈ β-W_2C > α-W_2C > c-WC > γ-W_2C_1, which is consistent with the observed trend of Young's modulus and shear modulus as shown in Table 4 Combining the values ofΘ_D and the Young's modulus, we may conclude that the mechanical stability and thermal stability of h-WC is the best one among all W–C compounds.

Besides, since the tungsten carbides studied in the present paper have metallic feature at the Fermi level, the calculations for the electronic structures and elastic constants enable us to estimate the heat capacity (c_p) at the low-temperature, which is given as

$$c_p(T) = \gamma T + \beta T^3 \quad (28)$$

$$\gamma = \frac{1}{3}\pi^2 k_B^2 D_f \quad (29)$$

$$\beta = \frac{12\pi^4 Rn}{5\Theta_D^3} \quad (30)$$

In the equations, γ and β are the coefficients of electronic and lattice heat capacities, respectively; n is the total number of atoms per formula unit and R is the molar gas constant. Heat capacity is an invaluable tool to explore the fundamental properties of materials. Note that Θ_D, as a rule, only describes the temperature dependence of c_p for $T < \Theta_D/10$ [63]. Therefore, In Fig. 6, we plot c_p versus T in the 0–50 K temperature range for all W–C compounds. At temperatures up to 9 K, as can be seen from Fig. 6, the main contribution to c_p is the excitation of electrons, and the values of c_p have the following sequence: h-WC < c-WC < γ-W_2C_2 ≈ β-W_2C < α-W_2C < ε-$W_{2s}C$ < γ-W_2C_1, which are as same as the sequences of γ indicating the heat capacities are determined by electrons at first; besides, in Table 7, the smallest value of γ = 0.36 mJ/(K^2·mol) is attributed to h-WC, because it has the smallest DOS value at the Fermi level, so h-WC has weakest metallic nature among all W–C compounds. In the range of 9–50 K, contributions from phonon excitations must be taken into account, as a result, the growth trend of c_p is: h-WC < c-WC < γ-W_2C_2 ≈ β-W_2C < ε-W_2C < α-W_2C < γ-W_2C_1. Thus, we can conclude that the heat capacity from electrons dominates the c_p curve at first, when T further raises the heat capacity is determined by phonon excitations. In addition, in the literature [45], the authors reported the values of c_p for h-WC in a large temperature range of 50–500 K, when T = 50 K the value of 3.12 J/(K·mol) was achieved. Note that at T = 50 K the agreement between the work and the calculated

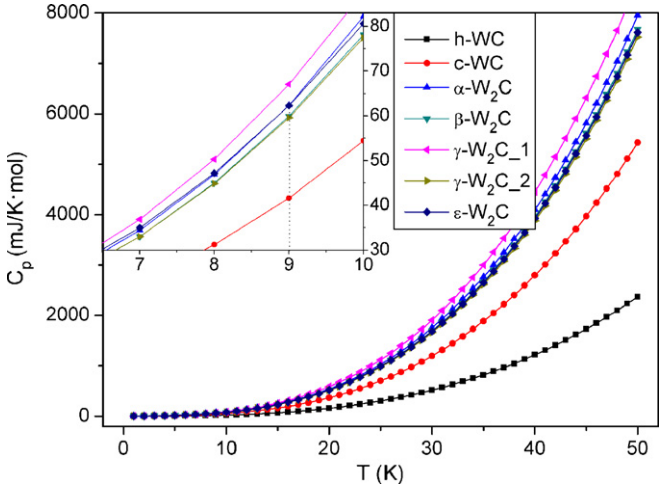

Fig. 6. Heat capacity of W–C compounds plotted in the range of 0–50 K.

results (2.39 J/(K·mol)) in our paper is pretty good. When $T > 50$ K, the variations of c_p follow the well-known rule, namely Debye's quasi-harmonic approximation. Unfortunately, similar experimental c_p data for other five W–C compounds are not available at the moment. This paper may be useful for low-temperature heat capacity research of W–C system compounds.

4. Conclusions

We used first-principles calculations to study the properties of W–C compounds. The Fermi level of h-WC is situated close to a minimum of the DOS that qualitatively indicates its stability nature; for c-WC, the Fermi level lies at the local maximum of DOS destabilizes the NaCl-like structure of WC, while all W_2C polymorphs have relatively large DOS values at the Fermi level, indicating they are less stable than h-WC. The calculated formation enthalpy values indicate that h-WC, β-W_2C, γ-W_2C_1, γ-W_2C_2 and ε-W_2C are thermodynamically stable, while c-WC and α-W_2C appear to be metastable or unstable. The calculated total electron density distribution maps clearly deduce the metallic nature of W–C compounds; since in all of these maps, even in the interstitial regions the electron density values are larger than zero. The elongated contours along W–C bond axis can be ascribed to the covalent interactions. From the population results, it is found that the charge transfer from W to C is significant. Therefore, the bonding behaviors of W–C compounds are combinations of covalent, metallic, and ionic nature. Based on the Stoner's polarization theory for itinerant magnetism, all of W–C binary compounds are in paramagnetic state. Moreover, we also calculated Pauli paramagnetic susceptibilities of them, and the results are in agreement with the available theoretical values.

The bulk modulus and the first pressure derivative are estimated by fitting the EOS for each compound. The bulk modulus of W–C system compounds is 400.9, 374.4, 343.3, 353.5, 343.9, 343 and 341.9 GPa for h-WC, c-WC, α-W_2C, β-W_2C, γ-W_2C and ε-W_2C, respectively, which exhibit larger values than the common carbides such as Cr_7C_3, Fe_3C, Cr_3C, and TiC; All W–C binary compounds are more incompressible than Cr_7C_3, Fe_3C, Cr_3C, TiC, etc. The full set of elastic constants is calculated for each compound based on strain–stress method using CASTEP code. The calculated elastic constants satisfy the Born–Huang's stability criterion, indicating that all these compounds are mechanically stable. The largest bulk modulus, shear modulus, and Young modulus are attributed to h-WC and the value is 393, 286.2, and 690.9 GPa, respectively. The calculated hardness values of h-WC and c-WC are smaller than that of W_2C polymorphs; this is mainly due to the less coordination numbers of atom W for α-W_2C, β-W_2C, γ-W_2C and ε-W_2C. The Debye temperature and heat capacity for these compounds are also calculated, the agreement between our results and other references is pretty good.

Acknowledgments

The authors appreciate Dr. X.J. Xie for useful discussion and thank to Prof. Y.H. Chen for providing a SGI working station and the CASTEP code. This research is supported by the Natural Science Foundation of China (no. 50872109), the 863 project in China (no. 2009AA03Z524), theCooperation Foundation for Industry, University and Research Institute, Guangdong Province and Ministry of Education of China (no. 2008B090500242), and the Economic and Trade Commission Creative Technology Program, Guangdong Province of China (no. 200872215).

References

[1] Y. Torres, M. Anglada, L. Llanes, Int. J. Refract. Met. Hard Mater. 19 (2001) 341.
[2] U. Beste, T. Hartzell, H. Engqvist, N. Axén, Wear 249 (2001) 324.
[3] C. Karatas, B.S. Yilbas, A. Aleem, M. Ahsan, J. Mater. Process. Technol. 183 (2007) 234.
[4] K. Bonny, P. De Baets, W. Ost, S. Huang, J. Vleugels, W. Liu, B. Lauwer, Int. J. Refract. Met. Hard Mater. 27 (2009) 350.
[5] A.S. Chaus, M. Hudáková, Wear 267 (2009) 1051.
[6] M. Pellizzari, D. Cescato, M.G. De Flora, Wear 267 (2009) 467.
[7] M. Wiefssner, M. Leisch, H. Emminger, A. Kulmburg, Mater. Charact. 59 (2008) 937.
[8] A.Y. Liu, R.M. Wentzcovitch, M.L. Cohen, Phys. Rev. B 38 (1988) 9483.
[9] V.P. Zhukov, V.A. Gubanov, Solid State Commun. 56 (1985) 51.
[10] D.J. Siegel, L.G. Hector, J.B. Adams, Surf. Sci. 498 (2002) 321.
[11] C.G. Larsson, J.B. Pendry, L.I. Johansson, Surf. Sci. 162 (1985) 19.
[12] P.M. Stefan, M.L. Shek, W.E. Spicer, Surf. Sci. 149 (1985) 423.
[13] F. Marinelli, A. Jelea, A. Allouche, Surf. Sci. 601 (2007) 578.
[14] D. Lou, J. Hellman, D. Luhulima, J. Liimatainen, V.K. Lindroos, Mater. Sci. Eng. A 340 (2003) 155.
[15] A. Antoni-Zdziobek, J.Y. Shen, M. Durand-Charre, Int. J. Refract. Met. Hard Mater. 26 (2008) 372.
[16] R.H. Willens, E. Buchler, Appl. Phys. Lett. 7 (1967) 25.
[17] M. Rajagopalan, P. Saigeetha, G. Kalpana, B. Palanivel, Jpn. J. Appl. Phys. 33 (1994) 1847.
[18] A.S. Kurlov, A.I. Gusev, Russ. Chem. Rev. 75 (2006) 617.
[19] D.V. Suetin, I.R. Shein, A.L. Ivanovskii, J. Phys. Chem. Solids 70 (2009) 64.
[20] D.V. Suetin, I.R. Shein, A.S. Kurlov, A.I. Gusev, A.L. Ivanovskii, Phys. Solid State 50 (2008) 1420.
[21] A. Klimpel, L.A. Dobrzański, A. Lisiecki, D. Janicki, J. Mater. Process. Technol. 164 (2005) 1068.
[22] T. Li, Q.F. Li, J.Y.H. Fuh, P.C. Yu, C.C. Wu, Mater. Sci. Eng. A 430 (2006) 113.
[23] M.F. Morks, Y. Gao, N.F. Fahim, F.U. Yinquing, Mater. Lett. 60 (2006) 1049.
[24] M.D. Segall, J.D. Philip, M.J. Lindan, C. Probert, J. Pickard, P.J. Hasnip, S.J. Clark, M.C. Payne, J. Phys.: Condens. Matter 14 (2002) 2717.
[25] A.E. Mattsson, P.A. Schultz, M.P. Desjarlais, T.R. Mattsson, K. Leung, Modell. Simul. Mater. Sci. Eng. 13 (2005) R1.
[26] L.Z. Cao, J. Shen, N.X. Chen, J. Alloys Compd. 336 (2002) 18.
[27] J.P. Perdew, K. Burke, Y. Wang, Phys. Rev. B 54 (1996) 16533.
[28] H.J. Monkhorst, J.D. Pack, Phys. Rev. B 13 (1976) 5188.
[29] S.N. Mishra, Phys. Rev. B 77 (2008) 224402.
[30] T. Beuerle, K. Hummler, C. Elsässer, M. Fähnle, Phys. Rev. B 49 (1994) 8802.
[31] K. Willenborg, R. Zeller, P.H. Dederichs, Europhys. Lett. 18 (1992) 263.
[32] S. Blügel, Phys. Rev. Lett. 68 (1992) 851.
[33] S. Stadler, R.P. Winarski, J.M. Maclaren, D.L. Ederer, J. canEk, A. Moewes, M.M. Grush, T.A. Callcott, R.C.C. Perera, J. Electron Spectrosc. Relat. Phenom. 110–111 (2000) 75.
[34] N.I. Medvedeva, A.L. Ivanovskii, Phys. Solid State 43 (2001) 469.
[35] D.L. Price, B.R. Cooper, Phys. Rev. B 39 (1989) 4945.
[36] J.R. Kitchin, J.K. Nørskov, M.A. Barteau, J.G. Chen, Catal. Today 105 (2005) 66.
[37] B. Xiao, J.D. Xing, J. Feng, C.T. Zhou, Y.F. Li, W. Su, X.J. Xie, Y.H. Cheng, J. Phys. D: Appl. Phys. 42 (2009) 115415.
[38] W. Zhou, L. Liu, B. Li, P. Wu, Q. Song, Comput. Mater. Sci. 46 (2009) 921.
[39] S.K.R. Patil, S.V. Khare, B.R. Tuttle, J.K. Bording, S. Kodambaka, Phys. Rev. B 73 (2006) 104118.
[40] Z.J. Wu, E.J. Zhao, H.P. Xiang, X.F. Hao, X.J. Liu, J. Meng, Phys. Rev. B 76 (2007) 054115.
[41] D.V. Suetin, I.R. Shein, A.L. Ivanovskii, Physica Status Solidi B 245 (2008) 1590.
[42] I.R. Shein, D.V. Suetin, A.L. Ivanovskii, Tech. Phys. Lett. 34 (2008) 841.
[43] M. Lee, R.S. Gilmore, J. Mater. Sci. 17 (1982) 2657.
[44] T. Sahraoui, A. Kellou, H.I. Faraoun, N. Fenineche, H. Aourag, C. Coddet, Mater. Sci. Eng. B 107 (2004) 1.
[45] R.R. Reeber, K. Wang, J. Am. Ceram. Soc. 82 (1999) 192.
[46] V.V. Brazhkin, A.G. Lyapin, R.J. Hemley, Philos. Mag. A 82 (2002) 31.
[47] M. Nikolussi, S.L. Shang, T. Gressmann, A. Leineweber, E.J. Mittemeijer, Y. Wang, Z.K. Liu, Scripta Mater. 59 (2008) 814.
[48] J.H. Jang, I.G. Kim, H.K.D.H. Bhadeshia, Comput. Mater. Sci. 44 (2009) 1319.
[49] D. Music, U. Kreissig, R. Mertens, J.M. Schneider, Phys. Lett. A 326 (2004) 473.
[50] Y. Yang, H. Lu, C. Yu, J.M. Chen, J. Alloys Compd. 485 (2009) 542.
[51] J.J. Gilman, B.W. Roberts, J. Appl. Phys. 32 (1961) 1405.
[52] Y.C. Liang, W.L. Guo, Z. Fang, Acta Physica Sin. 56 (2007) 4847.
[53] Z.L. Liu, X.R. Chen, Y.L. Wang, Physica B 381 (2006) 139.
[54] R.C.D. Richardson, Wear 10 (1967) 291.
[55] A. Šimůnek, J. Vackář, Phys. Rev. Lett. 96 (2006) 085501.
[56] A. Šimůnek, Phys. Rev. B 75 (2007) 172108.
[57] D.M. Teter, MRS Bull. 23 (1998) 22.
[58] F.M. Gao, Phys. Rev. B 73 (2006) 132104.
[59] F.M. Gao, J.L. He, E.D. Wu, S.M. Liu, D.L. Yu, D.C. Li, S.Y. Zhang, Y.J. Tian, Phys. Rev. B 91 (2003) 015502.
[60] E. Deligoz, Y.O. Ciftci, P.T. Jochym, K. Colakoglu, Mater. Chem. Phys. 111 (2008) 29.
[61] G.V. Sin'ko, N.A. Smirnow, J. Phys.: Condens. Matter 14 (2002) 6989.
[62] O.L. Anderson, J. Phys. Chem. Solids 24 (1963) 909.
[63] M.K. Drulis, A. Czopnik, H. Drulis, J.E. Spanier, A. Ganguly, M.W. Barsoum, Mater. Sci. Eng. B 119 (2005) 159.
[64] Y.A. Chang, L.E. Toth, Y.S. Tyan, Metall. Mater. Trans. B2 (1971) 315.